

# Admittance Control of an Upper Limb Exoskeleton – Reduction of Energy Exchange

Hyunchul Kim, Levi Makaio Miller, Zhi Li, Jay Ryan Roldan and Jacob Rosen

**Abstract**—The synergy of human arms and wearable robot systems (e.g. exoskeletons) is enabled by a control algorithm that maximizes the transparency between the two subsystems. The transparency can be improved by integrating the admittance control along with an arm redundancy resolution algorithm. Recent research effort resulted in a new criterion for the human arm redundancy resolution for unconstrained arm motions estimating the swivel angle with prediction errors of less than  $5^\circ$ . The proposed criterion for the arm redundancy resolution defines the mouth as the primary target of the the human hand during unconstrained arm motions in free space. It was postulated based on experimental data analysis that this criterion is based on a neural mechanism directing the hand towards the head for self-feeding. In conjunction with the proposed redundancy resolution criteria a task space admittance control algorithm is introduced based on multiple force sensor inputs obtained at the interface between the human arm and the exoskeleton system. The system performance was evaluated by five healthy subjects performing a peg-in-hole task for three different target locations. The velocities and interaction forces at the upper arm, lower arm, handle and tip were recorded and further used to power exchange between the subject and the device. Results indicated that the proposed control scheme outperforms the purely reactive task space admittance control with energy exchange reduced to 11.22%. Improving the quality of the human control of a wearable robot system may allow the robot to be a natural and transparent extension of the operator’s body.

## I. INTRODUCTION

The synergy between human arms and wearable robot systems (e.g. the exoskeletons) enables robots to enhance, support, and assist humans’ physical capabilities and motor control. In particular, assistive wearable robots [1][2] help people who suffer from a variety of neuromuscular diseases [3]. Healthy humans have flexible arm movement to manipulate objects and to avoid obstacles, while the robotic manipulators can augment power and reduce the fatigue due to heavy loads. By constructively combining the flexibility of natural human movements with the power of manipulation of the robots, we expect to achieve synchronized movements that minimize the energy exchange between the wearable robots and their human users and therefore improve the transparency of the human-robot system.

Over the past several decades, a number of important research efforts have resulted in improved synergy between wearable robot systems and their human users, either by improving the mechanical design of the wearable robots or by improving the underlying human machine interface (HMI). The first generation of the wearable exoskeleton robot, known as Hardiman, is developed for power

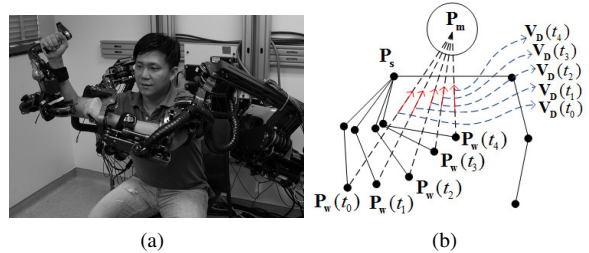


Fig. 1. a) The seven-DOF exoskeleton supports 99% of the ranges of motion required to perform daily activities. b) Virtual destination for the given wrist position at any time  $t_i$ .  $V_D(t_i)$  means the virtual destination formed at any time  $t_i$  depending on the wrist position  $P_w(t_i)$ .

augmentation [4][5]. It is controlled by position signals so that responsiveness and stability is not satisfactory. The second generation of exoskeletons are controlled by force signals that reflected the human’s intention on the robot at the dynamic level. This improvement in control strategy enabled the operators to have full physical contact with the exoskeleton during manipulation [6][7][8]. Several extender prototypes are designed and built in order to study the control by force single. However, these wearable robots are unable to comply with their human users, and the reactive forces of largely reduced the flexibility of human motion.

Recent research has focused on the transparency of the human-robot system so that the operator feels less reaction from the wearable robot [9][10]. In particular, this research effort intends to develop a control strategy for an upper limb exoskeleton with seven degrees of freedom (DOFs), so that it renders natural arm postures. The proposed admittance controller integrates a motion prediction algorithm that determines the joint configurations of the exoskeleton based on a new kinematic constraint. The force interaction between the wearable robot and the user is extracted via four force sensors allocated on the wearable robot, such that the exoskeleton can render flexible movements for sophisticated tasks. The proposed admittance controller is compared to a purely reactive admittance controller by the performance on a peg-in-hole task.

## II. SYSTEM MODEL AND METHOD

### A. Exoskeleton Design

The kinematics and dynamics of the human arm during activities of daily living (ADL) have been studied to determine the specifications for the exoskeleton design [Fig. 1(a)] [1][11]. Articulation of the exoskeleton is achieved by seven single-axis revolute joints which support 99% of the range of motion required to perform daily activities [1]. Three revolute joints are responsible for shoulder abduction-adduction, flexion-extension and internal-external rotation. The elbow has a single revolute joint for flexion-extension. The lower arm and hand are connected by a three-axis spherical joint resulting in wrist pronation-supination, flexion-extension, and

Hyunchul Kim Ph.D. is with the Dept. of Electrical Engineering, University of California Santa Cruz, Santa Cruz, CA  
e-mail: hyunchul78@gmail.com

Zhi Li M.Sc., Jay Ryan Roldan BS, and Jacob Rosen Ph.D. are with the Dept. of Computer Engineering, University of California Santa Cruz, Santa Cruz, CA

e-mails: zhil@soe.ucsc.edu, juoldan@ucsc.edu, rosen@ucsc.edu

Bionics Lab URL: <http://bionics.soe.ucsc.edu/>

Levi Makaio Miller Ph.D. is with the Dept. of Mechanical Engineering, University of Washington, Seattle WA makaio@uw.edu

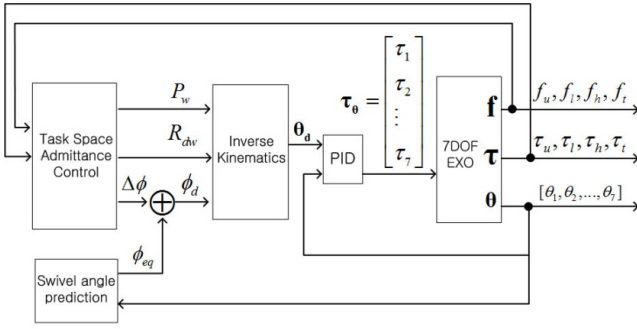


Fig. 2. Block diagram of proposed admittance controller.  $(f_u, \tau_u)$ ,  $(f_l, \tau_l)$ ,  $(f_h, \tau_h)$ ,  $(f_t, \tau_t)$  indicate the force/torque signal from four six-axis force/torque sensors attached to the upper arm, the lower arm, the handle and the tip of the exoskeleton robot hand respectively.

radial-ulnar deviation. As a human-machine interfaces (HMI), four six-axis force/torque sensors (ATI Industrial Automation, model-Mini40) are attached to the upper arm, the lower arm, the hand and the tip of the exoskeleton [12]. Since even small differences in the exoskeleton position and the user's desired position can cause discomfort, additional force sensors at the upper and lower arm to track the interactions of the user and the device. At the upper and lower arm of the exoskeleton, the force/torque sensors are attached to a pressure distributive structural pad that securely straps to the mid-distal portion of each arm segment; while at the hand of the exoskeleton, the force/torque sensor is integrated with the handle. The interactions between the exoskeleton and the user are measured via those force/torque sensors. The force/torque sensor at the tip of the exoskeleton also measures the interactions between the exoskeleton and the environment.

### B. Overall Admittance Control Scheme

The overall admittance control scheme is described in Fig. 2. Due to the redundancy in the seven-DOF robotic system, not only the handle but also the elbow angle velocity should be considered in the control. The wrist position and orientation are calculated independently in task space using the four force sensors. The desired swivel angle  $\phi_d$  is the combination of predicted swivel angle,  $\phi_{eq}$  representing the natural arm posture, and deviation of the swivel angle  $\Delta\phi$  from the  $\phi_{eq}$  based on the force sensors. The wrist position  $P_w$  and orientation  $R_{dw}$  together with the swivel angle  $\phi_d$  are fed through the inverse kinematic function [12] to create  $\Theta_d = \{\theta_{1d}, \theta_{2d}, \dots, \theta_{7d}\}$ . A PID control is then used to track joint trajectories. The predicted swivel angle immediately provides the natural arm movement for the simple reaching-grabbing task to overcome the limitation of the purely reactive admittance control with relatively high energy exchanges between human and robot.

## III. ADMITTANCE CONTROL WITH MOTION PREDICTION

This section describes the swivel angle prediction algorithm based on a proposed kinematic constraint [13] and the force feedback.

### A. Swivel Angle $\phi_{eq}$ Prediction Based on Biological Need

The arm model with seven degrees of freedom is redundant with respect to the six degrees of freedom 3D task space, and controlling the extra degree of freedom is critical in rendering natural human arm movements on the exoskeleton. Given the position (three DOFs

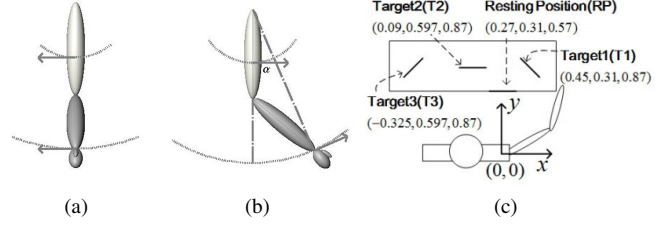


Fig. 3. Force interactions at the upper arm create motion that is tangent to a sphere that is centered at the shoulder. (a) The x component of an upper arm force creates motion in the x direction at the upper arm and wrist. (b) The y component of the force creates a motion in the y direction at the upper arm but the motion is rotated by  $\alpha$  at the wrist. The z component is resisted by the mechanism and does not result in motion. (c) Target location for the admittance control algorithm test with respect to the Exo position.

in x, y and z direction) and orientation (three DOFs about x, y and z direction) of the end-effector, it is convenient to represent the extra DOF by the swivel angle as [13], which presented a kinematic constraint based biological need of feeding to account for the natural human arm movements.

### B. Swivel Angle $\Delta\phi$ Based on a Force Feedback

1) *Wrist Position*: Forces at the tip ( $\vec{f}_t$ ), handle ( $\vec{f}_h$ ) and lower arm ( $\vec{f}_l$ ) are related to the position change of the wrist. Motions of the device due to the interaction forces are in the same direction as the force vector. However, the spherical joint of the shoulder constrains any point on the upper arm to the surface of a sphere. Thus a force applied on the upper arm is tangential to the shoulder sphere and the perpendicular force component to the sphere is resisted by the device. Let's define a frame at the origin of the upper arm force sensor. This frame has x, y and z axis pointing to the user's right, forward and up when the arm is at the side. The z component of the upper arm force is zero since it is perpendicular to the sphere of motion. The x component creates different motion at the wrist according to the elbow rotation angle. When the vectors tangent to the surface of the spheres at the wrist and upper arm are separated by the angle  $\alpha$  as shown in Fig. 3(a), the original upper force signal ( $\vec{f}_u$ ) gets transformed as follows:

$$\vec{f}_u = \begin{bmatrix} x \\ y \\ z \end{bmatrix} \Rightarrow \begin{bmatrix} x \\ y \\ 0 \end{bmatrix} \Rightarrow \begin{bmatrix} x \\ \cos(\alpha)y \\ \sin(\alpha)y \end{bmatrix} \quad (1)$$

The four sets of force signals are transformed based on  $\vec{f}' = R_1 R_2 \dots R_n \vec{f}$  for coordination in a common frame.  $\vec{f}$  is the force measurement.  $n$  is the link frame to which the sensor is attached.  $\vec{f}'$  is the force represented in the global frame. Since the force between the user and the exoskeleton device should be zero in an ideal case, the error in the force ( $\vec{f}_e$ ) will be  $\vec{f}_e = \vec{f}'_u + \vec{f}'_l + \vec{f}'_h + \vec{f}'_t - \vec{0}$  with zero as reference force. Next, we transform the force signals into a task space position signal.

$$x = k_p \vec{f}_e + k_i \int \vec{f}_e - k_d \dot{x} \quad (2)$$

The last term ( $-k\dot{x}$ ) is from Hook's Law [14] for an approximate derivative of the noisy force signal.

2) *Wrist Orientation*: Changes in the wrist orientation are calculated based on torque at the wrist. The handle and tip force sensor will produce torques at the wrist. Since neither the wrist sensor nor the tip sensors are located at the wrist, the torque at the wrist ( $\vec{\tau}_w$ ) due to the handle will be the addition of the handle torque ( $\vec{\tau}_h$ ) with the cross product of the handle distance ( $\vec{r}_h$ ) and the handle force

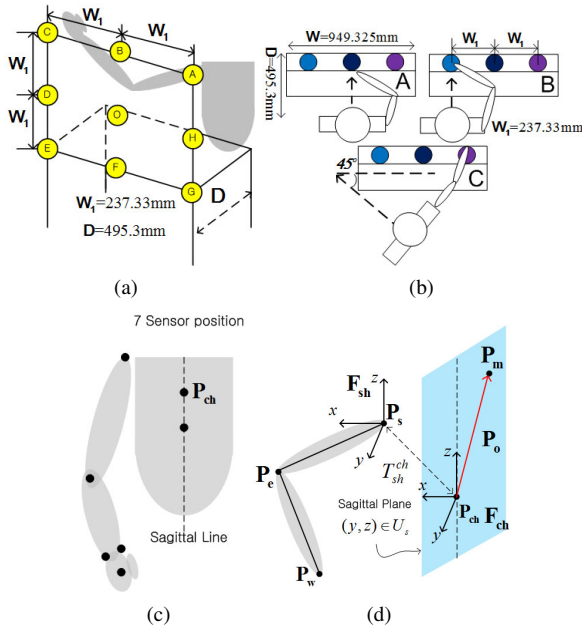


Fig. 4. (a) Hand trajectory for data collection. (b) Top view of three different tasks. Height of table-top to top-of-shelf = 501.65mm, Height of table-top from ground = 736.6mm. (c) Positions of LED markers: the shoulder (acromioclavicular joint), the elbow (lateral edge of the ulna), the wrist (medial & lateral edge of the distal end of the radius & ulna), palm (between 2 & 3 metacarples) and Torso(Upper & lower sternum). (d)  $P_m$  location with respect to the  $P_{ch}$ .

( $\vec{f}_h$ ). Similarly, the torque at the wrist due to the tip will be the tip torque ( $\vec{\tau}_t$ ) plus the cross product of the tip distance ( $\vec{r}_t$ ) with the tip force ( $\vec{f}_t$ ). The total torque at the wrist will be the addition of the contributions of the handle and the tip. Next, we transform  $\vec{\tau}_w$  from the sensor frame into the global frame.

$$\vec{\tau}_w = \left[ \vec{\tau}_h + (\vec{r}_h \times \vec{f}_h) \right] + \left[ \vec{\tau}_t + (\vec{r}_t \times \vec{f}_t) \right] \quad (3)$$

$$\vec{\tau}_w' = R_1 R_2 R_3 R_4 R_5 R_6 R_7 \vec{\tau}_w \quad (4)$$

The desired reference torque is zero, making the error signal  $\vec{\tau}_e = \vec{\tau}_w' - \vec{0}$ . Taking  $\vec{\tau}_e$  to be the axis angle representation for the change in orientation, a rotation matrix ( $R_e$ ) can be constructed to represent the desired change.

$$\theta_e = \|\vec{\tau}_e\| \quad (5)$$

$$\vec{\omega}_e = \frac{\vec{\tau}_e}{\theta_e} \quad (6)$$

$$R_e = I + \hat{\omega}_e \sin(\theta_e) + \hat{\omega}_e^2 (1 - \cos(\theta_e)) \quad (7)$$

where  $\theta_e$  is the desired change in angle,  $\vec{\omega}_e$  is the rotation axis,  $I$  is the  $3 \times 3$  identity matrix, and  $\hat{\omega}_e$  is the antisymmetric matrix equivalent of the cross product. With this, the desired orientation ( $R_d$ ) becomes  $R_d = R_e R_{d-1}$ , where  $R_{d-1}$  is the desired orientation from the previous time step. At initiation  $R_{d-1}$  is set equal to the current orientation of link 7.

3) *Swivel Angle from Admittance Control*: Changes in the swivel angle are calculated based on the torque on the swivel axis. In our case, only the upper and lower arm forces contribute to the torque around the swivel axis. The upper and lower arm sensors are measured in different frames and must be coordinated in a common global frame. Then the total torque on the shoulder ( $\vec{\tau}_s$ ) is the addition of the contributions from the upper and lower arm.

$$\vec{\tau}_s = \left[ \vec{\tau}_u' + (\vec{r}_u \times \vec{f}_u') \right] + \left[ \vec{\tau}_l' + (\vec{r}_l \times \vec{f}_l') \right] \quad (8)$$

where  $\vec{\tau}_u'$  and  $\vec{f}_u'$  are the torque and force at the upper sensor. Then similarly  $\vec{\tau}_l'$  and  $\vec{f}_l'$  are the torque and force at the lower arm. Only the component of torque that acts on the swivel axis will cause a change in the swivel angle. Thus the component of  $\vec{\tau}_s$  acting on the normal vector  $\vec{n}$  pointing from should position ( $P_s$ ) to wrist position ( $P_w$ ) is  $\vec{\tau}_n = \vec{\tau}_s \cdot \vec{n}$ . The desired reference torque is zero so the error is equal to  $\vec{\tau}_e = \vec{\tau}_n - 0$  and the desired swivel angle change is:

$$\Delta\phi = k_p \vec{\tau}_e + k_i \int \vec{\tau}_e - k_d \dot{\vec{\tau}}_e \quad (9)$$

where the term  $(-k_d \dot{\vec{\tau}}_e)$  is similarly defined as Eq. 2.

## IV. EXPERIMENT AND PERFORMANCE ANALYSIS

### A. Experimental System and Protocol for $\phi_{eq}$ Evaluation

The experimental setup is shown in Fig. 4. The kinematic data of the human arm is collected using a motion capture system (Phasespace, Inc.) equipped with eight cameras, providing a 240Hz sampling rate and a millimeter accuracy at a distance of three meters. To record each joint movement, active LED markers were attached to key anatomical locations: shoulder, elbow, wrist and chest [Fig. 4(c)].

Five right-handed healthy subjects (three male and two female with average height and age of 175 cm and 29 respectively) participated in the experiment. Each subject was asked to reach nine different target locations sequentially at a self-directed pace as follows [Fig. 4(a)]:

$$O \rightarrow A \rightarrow B \rightarrow C \rightarrow D \rightarrow E \rightarrow F \rightarrow G \rightarrow H (5 \text{ repetitions})$$

Subjects repeated each sequence five times in three different body orientations (A, B, and C, shown in Fig. 4(b)). In orientation A, the center of the subject's chest was aligned with the center of the targets. In orientation B, the center of the subject's chest was aligned with the leftmost targets. And in orientation C, the subject's body is rotated counterclockwise by 45 degrees. The experiment covers the majority of the right arm workspace.

### B. Precision of $\phi_{eq}$ Estimation Algorithm

Table. I shows the comparison between the biologically-based kinematic constraint swivel angle  $\phi_{eq}$  prediction and the calculated swivel angle generated by healthy subjects during reaching movements. It is shown that the mean of the absolute error is less than five degrees and the standard deviation is less than four degrees.

TABLE I  
ESTIMATION ERROR

Subject	$P_o(mm)$ ( $y_{opt}, z_{opt}$ )	Standard Deviation of Error			Mean error
		Exp 1	Exp 2	Exp 3	
1	(-160,280)	2.344°	2.720°	3.769°	3.024°
2	(-140,320)	2.337°	2.579°	1.365°	3.516°
3	(-70,290)	3.395°	2.756°	2.340°	4.103°
4	(-140,330)	2.817°	2.564°	3.010°	3.525°
5	(-60,220)	2.740°	3.225°	3.501°	4.739°

### C. Performance of the Proposed Admittance Control

The proposed admittance controller is compared with the purely reactive admittance control algorithm that is not using  $\phi_{eq}$ . The interaction power, interaction energy, and completion time are calculated for each reaching task performed wearing the exoskeleton.

The interaction power is calculated by adding all translational and rotational portion of the power at each attachment point(total

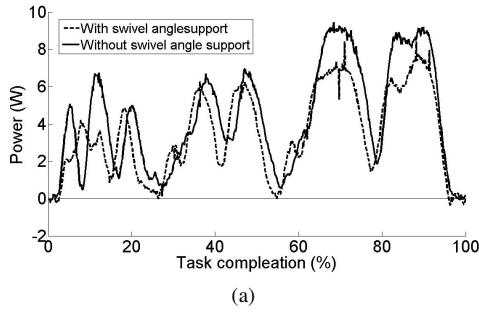


Fig. 5. The interaction power of the exoskeleton averaged over the users.

of 4 force/torque sensors each arm). Translational power is obtained by taking the dot product of the force sensor data and the velocity calculated using the forward kinematic map and joint position data. Similarly, the rotational power is obtained as the dot product of the torque, recorded from the force sensors, with the angular velocity calculated using the joint position sensors and the forward kinematic map. Interaction energy is found by taking the integral of the power. The completion time is recorded between when the brake pedal for the robot is first pressed to when the pedal is released.

#### D. Experiment Setup to Evaluate the Proposed Admittance Control

The exoskeleton's height is adjusted for each individual subject in a seated position. The subject is secured in the device with the two straps, one at the upper arm and the other at the lower arm. In front of the subject is a table with three target plates. The targets are numbered 1 to 3 from the subject's right to left. The locations of the targets are defined in Fig. 3(c) as a meter scale. Note that  $z$  points up and is measured from the floor. Each subject is instructed to touch the target in the following order.

$$RP \rightarrow T1 \rightarrow RP \rightarrow T2 \rightarrow RP \rightarrow T3 \rightarrow RP(20\text{times}) \quad (10)$$

#### E. Result

The average power profile for all subjects in Fig. 5(a) shows that the power peaks correspond to pushing the exoskeleton towards or pulling back from targets, and the valleys occur when the subjects approach to the target and their velocities are reduced. The approaching and retraction for each target is clearly distinguishable in the plot: the further the target location, the greater the interaction power. Thus, it is expected that as the further the target position, the more time the arm need for acceleration. Fig. 5(a) also shows that although the power profile for control with and without swivel support are similar, the peaks and valleys are lower when swivel support is on. The interaction energy averaged over all subjects showed a statistically significant difference (at the .05 level) depending if swivel support is used. The task interaction energy is 42.07 J with swivel support and 46.79 J without swivel support, indicating an 11.22% increase in the positive energy interaction if swivel support is not used. It is important to note that the interaction energy is the energy exchange between the robot and user. It contains no information about the total energy of either system to complete the task. Thus, there is no statistically significant difference in the completion time with additional swivel angle support.

#### V. CONCLUSION

We introduced a new admittance control scheme combining the prediction of the natural arm posture with the purely reactive force-sensor-based admittance control. The redundancy of the human arm

in a simple reaching task is estimated from a new inverse kinematic constraint and the deviation from the natural arm postures are made by converting force and torque to the desired changes in the joint angles. The proposed arm prediction model is computationally efficient and precise having less than  $5^\circ$  error such that it is applicable to realtime control. The performance of the proposed algorithm is also compared with a purely reactive task space admittance control and it is shown that the energy exchange between human and robot is reduced by 11.22%

#### REFERENCES

- [1] J. C. Perry, J. Rosen, and S. Burns, "Upper-limb powered exoskeleton design," *Mechatronics*, vol. 12, no. 4, pp. 408–417, 2007.
- [2] T. Nef, M. Guidali, V. Klamroth-Marganska, and R. Riender, "Design of a 7 degree-of-freedom upper-limb powered exoskeleton," in *World Congress on Medical Physics and Biomedical Engineering IFMBE*, vol. 25/9, Munich, Germany, Sept 2009.
- [3] H. I. Krebs, M. Ferraro<sup>3</sup>, S. P. Buerger<sup>1</sup>, M. J. Newbery<sup>1</sup>, A. Makiyama, M. Sandmann, D. Lynch<sup>3</sup>, B. T. Volpe, and N. Hogan<sup>1</sup>, "Rehabilitation robotics: pilot trial of a spatial extension for mit-manus," *Journal of NeuroEngineering and Rehabilitation*, Oct 2004.
- [4] G. E. Company, "Hardiman I prototype project, special interim study," no. S-68-1060, 1968.
- [5] B. J. Makinson, "Research and development prototype for machine augmentation of human strength and endurance, hardiman I project," no. S-71-1056, 1971.
- [6] A. B. Zoss, H. Kazerooni, and A. Chu, "Biomechanical design of the berkeley lower extremity exoskeleton (bleex)," *IEEE/ASME Transactions on Mechatronics*, vol. 11, no. 2, 2006.
- [7] H. Kazerooni and R. Steger, "The berkeley lower extremity exoskeleton," *Dynamic Systems, Measurements, and Control*, vol. 128, pp. 14–25, 2006.
- [8] H. Kazerooni, R. Steger, and L. Huang, "Hybrid control of the berkeley lower extremity exoskeleton (bleex)," *The International Journal of Robotics Research*, no. 5-6, pp. 561–573, 2006.
- [9] K. Sakita, K. Ogawara, S. Murakami, K. Kawamura, and K. Ikeuchi, "Flexible cooperation between human and robot by interpreting human intention from gaze information," in *Proceedings. 2004 IEEE/RSJ Int. Conf. on Intelligent Robot and Systems*, Sept 2004, pp. 846–851.
- [10] C. Fleischer, C. Reinicke, and G. Hommel, "Predicting the intended motion with emg signals for an exoskeleton orthosis controller," in *Proceedings. 2005 IEEE/RSJ Int. Conf. on Intelligent Robot and Systems*, Aug 2005, pp. 2029–2034.
- [11] J. C. Perry and J. Rosen, "Design of a 7 degree-of-freedom upper-limb powered exoskeleton," in *IEEE/RAS-EMBS International Conference on Biomedical Robotics and Biomechanics*, Pisa, Italy, Feb 2006.
- [12] L. M. Miller and J. Rosen, "Comparison of multi-sensor admittance control in joint space and task space for a seven degree of freedom upper limb exoskeleton," in *IEEE/RAS-EMBS International Conference on Biomedical Robotics and Biomechanics*, Tokyo, Japan, Sept 2010.
- [13] H. Kim, L. Miller, and J. Rosen, "Redundancy resolution of a human arm for controlling a seven dof wearable robotic system," in *IEEE international conference on EMBC*, Boston, USA, August 30 September 3 2011.
- [14] H. Seraji, "Adaptive admittance control: An approach to explicit force control in compliant motion," in *Proceedings of the IEEE International Conference on Robotics and Automation*, 1994, pp. 2705–2712.